

Sigil: Server-Enforced Watermarking in U-Shaped Split Federated Learning via Gradient Injection

Zhengchunmin Dai*, Jiaxiong Tang*, Peng Sun[†], Honglong Chen[‡], and Liantao Wu*

*Software Engineering Institute, East China Normal University

[†]College of Computer Science and Electronic Engineering, Hunan University

[‡]College of Control Science and Engineering, China University of Petroleum (East China)

{51275902069, 51275902027}@stu.ecnu.edu.cn,

psun@hnu.edu.cn, chenhl@upc.edu.cn, ltwu@sei.ecnu.edu.cn

Abstract—In decentralized machine learning paradigms such as Split Federated Learning (SFL) and its variant U-shaped SFL, the server’s capabilities are severely restricted. Although this enhances client-side privacy, it also leaves the server highly vulnerable to model theft by malicious clients. Ensuring intellectual property protection for such capability-limited servers presents a dual challenge: watermarking schemes that depend on client cooperation are unreliable in adversarial settings, whereas traditional server-side watermarking schemes are technically infeasible because the server lacks access to critical elements such as model parameters or labels.

To address this challenge, this paper proposes *Sigil*, a mandatory watermarking framework designed specifically for capability-limited servers. *Sigil* defines the watermark as a statistical constraint on the server-visible activation space and embeds the watermark into the client model via gradient injection, without requiring any knowledge of the data. Besides, we design an adaptive gradient clipping mechanism to ensure that our watermarking process remains both mandatory and stealthy, effectively countering existing gradient anomaly detection methods and a specifically designed adaptive subspace removal attack. Extensive experiments on multiple datasets and models demonstrate *Sigil*’s fidelity, robustness, and stealthiness.

1. Introduction

Deep Neural Networks (DNNs) now represent the state-of-the-art for a wide array of computer vision tasks [1], [2], [3], powering critical applications from medical image analysis to autonomous driving. The development of these high-performance vision models requires a massive investment in curated datasets, extensive computational resources, and domain-specific expertise. Consequently, these trained models are not merely academic results; they are valuable Intellectual Property (IP) that embodies significant research effort and competitive advantage for the organizations that create them.

However, the high value of these models also makes them targets for attackers, leading to escalating issues of intellectual property rights infringement, such as model

leakage, unauthorized copying, and illicit distribution [4], [5]. To protect the ownership of DNN models, model watermarking techniques have been proposed and extensively studied. Specifically, existing DNN model watermarking is mainly divided into two categories: backdoor watermarking [6], [7] and parameter watermarking [8], [9], [10]. Backdoor watermarking schemes typically use a secret set of trigger samples to embed ownership information into the target model’s input-output behavior, which can later be verified through black-box queries on a suspicious model. In contrast, parameter watermarking schemes encode watermark information, such as a specific bit string, directly into the model’s parameter space, which requires white-box access to the model parameters for extraction and verification.

Meanwhile, driven by growing concerns for data privacy and security, decentralized machine learning (DCML) paradigms, such as Federated Learning (FL) [11], [12], Split Learning (SL) [13], [14], and their variants [15], [16], have experienced rapid development. These frameworks not only enhance privacy but also greatly broaden the scope of data collaboration and model deployment.

Nevertheless, DCML introduces unprecedented challenges for IP protection. On one hand, as training involves multiple participants, the potential points of model leakage multiply, exacerbating the risk of infringement [17], [18], [19]. On the other hand, the fundamental differences in computational capabilities, data visibility, and training workflows among participants render traditional DNN watermarking approaches ineffective or infeasible in many cases.

As the most mature field within DCML, FL has been extensively studied for its corresponding watermarking techniques. In a typical FL setting, a central server coordinates the global model without direct access to clients’ data, while multiple clients hold private datasets, labels, and local models. Consequently, FL watermarking methods are generally categorized as either client-side [20], [21], [22] or server-side [23], [24], each tailored to distinct security assumptions (e.g., a trusted server or trusted clients).

While the FL server’s lack of access to client data prevents the direct embedding of traditional backdoor watermarks, it still maintains control over the global model distributed in each round. This control enables the adap-

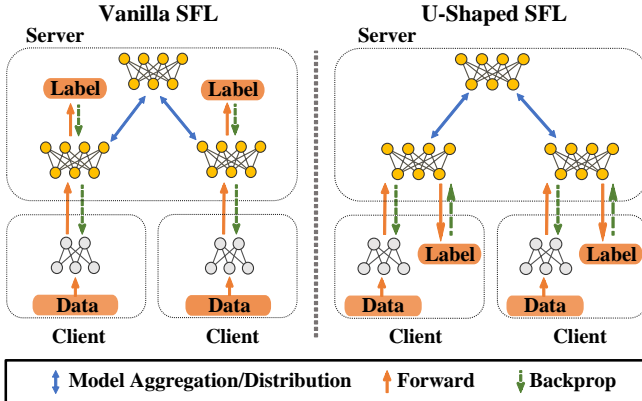


Figure 1. Comparison of Vanilla SFL and U-Shaped SFL Architectures.

TABLE 1. COMPARISON OF SERVER CAPABILITIES AND WATERMARK EMBEDDABILITY ACROSS FRAMEWORKS.

Server Capability	FL	SL/SFL	U-SL/U-SFL
Client Model Access	●	○	○
Client Labels Access	○	●	○
Client Data Access	○	○	○
Parameter Watermark	●	○	○
Backdoor Watermark	●	●	○

- Full Capability / Embedable
- Partial Capability / Partially Embedable
- No Capability / Not Embedable

tation of many traditional DNN watermarking techniques, such as embedding backdoor watermarks by substituting the required private data with public or noisy data [23], or directly embedding parameter watermarks [24]. Although these adaptations are feasible within FL, their dependence on global model access makes them fundamentally incompatible with SL.

SL [13], [14] is another emerging DCML paradigm that partitions a model into client-side and server-side components, thereby preserving client data privacy. U-shaped SL further enhances client privacy by also retaining the labels locally. These paradigms can be combined with FL to support multi-client scalability, forming Split Federated Learning (SFL) and U-shaped SFL (U-SFL) [15], [16].

In the U-SFL workflow (Figure 1), clients and the server collaboratively train their respective model segments. The client processes input data and sends intermediate activations (i.e., smashed data) to the server. The server completes the forward pass and, importantly, sends the output (logits) back to the client for loss computation, as the server lacks access to the labels. Gradients are then backpropagated. After several local epochs, the client-side and server-side model parameters are independently aggregated (i.e., via FedAvg) and redistributed for the next round.

While this architecture significantly enhances client privacy, it conversely exposes the server to severe model leakage risks. Recent research has shown that under a U-SFL

architecture, a malicious client can leverage the intermediate information, such as the returned logits, to successfully extract a high-accuracy replica of the server’s model using techniques like knowledge distillation. These works [17], [18], [19] highlight a significant and unresolved IP protection challenge in the U-SFL framework.

Addressing this threat using traditional model watermarking is challenging due to the server’s limited role in U-SFL. The server acts only as a coordinator for intermediate feature computation and gradient propagation. It lacks access to client data, labels, and model parameters, and cannot directly inspect or modify the client-side model. This restricted capability makes IP protection for the server both critical and difficult, placing traditional model watermarking techniques in a dual dilemma:

Dilemma One: Unreliability of client-side watermarking schemes. These methods rely on a semi-honest security assumption, requiring client cooperation during watermark embedding. However, a malicious client intent on model theft is unlikely to cooperate and may actively remove or circumvent the watermark.

Dilemma Two: Infeasibility of traditional server-side watermarking schemes. Conventional DNN or FL server-side watermarking methods presuppose server privileges such as direct modification of the global model or control over training data and labels. In U-SFL, the capability-limited server lacks these privileges, rendering such approaches technically infeasible.

This leads to a critical open question: *How can a capability-limited server, without access to any of the client’s private information such as data, labels, model parameters, forcibly embed a verifiable ownership credential into a potentially malicious client’s model?*

To address this challenge, this paper proposes *Sigil*, a mandatory watermarking framework designed specifically for capability-limited servers. *Sigil* leverages the gradient channel—the only channel under server control—to embed the watermark as a statistical constraint. This constraint enforces the server-visible activations, when projected into a randomly defined secret subspace, to match a target bit string. We further design an adaptive gradient clipping mechanism to enhance the stealthiness and robustness of this process against gradient anomaly detection and targeted adaptive attacks. To rigorously validate our approach, we build our threat model and perform evaluations under the U-SFL setting, where the server possesses minimal privileges.¹

We conduct extensive experimental evaluations on two representative datasets and four models. The experiments demonstrate that *Sigil* achieves high fidelity and strong stealthiness under two state-of-the-art (SOTA) gradient anomaly detection schemes. We also design a targeted adaptive subspace removal attack to further stress-test the framework, confirming its robustness against both conventional and advanced adaptive watermark removal attacks.

1. Our framework is general and can also be directly deployed in standard SL and SFL scenarios, where the server enjoys greater control, without any modifications.

In summary, the key innovations and contributions of this research are as follows:

- **Problem formalization.** We formalize the unique watermarking problem under the U-SFL paradigm by clearly defining the roles, capabilities, and threat model, where a trusted yet capability-limited server must embed a watermark into a potentially malicious client. We further identify the dual dilemmas that render existing watermarking schemes ineffective in this setting.
- **Framework Design.** We propose a general activation watermarking framework, *Sigil*, and design its watermark embedding and extraction mechanisms. *Sigil* repurposes the gradient channel—traditionally exploited for attacks—for IP protection, enabling a capability-limited server to perform mandatory watermark embedding without accessing any client-private information.
- **Adaptive Gradient Clipping.** We develop an adaptive gradient clipping mechanism to ensure the stealthiness and robustness of the watermarking process. This design allows *Sigil* to resist state-of-the-art gradient anomaly detection techniques and a tailored adaptive subspace removal attack, ensuring the enforceability of mandatory watermark embedding.
- **Comprehensive Evaluation.** Extensive experiments on two datasets and four model architectures validate the *fidelity*, *robustness*, and *stealthiness* of the *Sigil* framework under two state-of-the-art detection schemes. The implementation is publicly available at https://anonymous.4open.science/r/sfl_awm-EEFC/.

2. Related Work

This section first surveys existing watermarking approaches, including traditional DNN (backdoor, parameter, activation) and FL schemes. It then discusses the gradient anomaly detection challenges in SL that *Sigil* is designed to address.

2.1. Model Watermarking for IP Protection

DNN Watermarking. Model watermarking primarily includes backdoor watermarking [6], [7], [25], [26], [27], parameter watermarking [8], [9], [10], [28], [29], [30], [31] and activation watermarking [32]. Among them, backdoor watermarking embeds identity information into a model’s input–output behavior using a secret trigger set, while parameter watermarking encodes a secret bit string directly into the model’s parameter space. Both approaches rely on full control over the training data, labels, or model parameters—assumptions that are invalid in our U-SFL setting, where the server has no access to either data or client-side model weights.

Compared with the above two categories, activation watermarking is conceptually closer to our problem scenario. This approach embeds watermark information into

the activations of intermediate network layers, rather than into data or model parameters. A representative example is DeepSigns [32], which introduces a label-aware mechanism that embeds watermark information into preset class-center vectors, encouraging activations of samples from the same class to cluster around their corresponding centers. However, DeepSigns’ dependence on label information makes it incompatible with the U-SFL setting, where the server cannot access such information. Furthermore, as highlighted in a recent systematization-of-knowledge (SoK) study [33], DeepSigns faces limitations in fidelity, robustness, and scalability to complex tasks, making it insufficient for modern IP protection needs.

FL Watermarking. FL is the most extensively studied DCML paradigm. Existing FL watermarking research provides useful insights for distributed IP protection, yet the methods cannot be directly applied to U-SFL due to fundamental architectural and capability differences. FL watermarking schemes can be divided into client-side embedding and server-side embedding approaches.

Client-side embedding schemes [20], [21], [22] assume clients are trusted or semi-honest and perform watermark embedding locally. This assumption contradicts our malicious client threat model (defined in Section 3.1). A malicious client may refuse to embed a watermark and even attempt to remove or obfuscate it using full knowledge of the scheme.

Server-side embedding schemes, such as Waffle and FedTracker [23], [24], leverage the FL server’s authority to directly access, modify, and embed watermarks into the global model before distributing it in each training round. However, this design presupposes server access to the global model parameters—an assumption fundamentally incompatible with U-SFL, where the server has no visibility into client-side model components.

In summary, while existing watermarking schemes provide valuable foundations for model protection in distributed scenario, the restricted model partitioning and limited server capabilities in U-SFL necessitate a novel framework specifically tailored to this unique setting.

2.2. Gradient Channel Security in Split Learning

In SL and its variants, the activations uploaded by the client and the gradients returned by the server constitute the core channel for their interaction, which has consequently become the focus of SL security research.

On one hand, research has shown that this channel can be exploited by a malicious server. For example, FSHA and its variants [34], [35], [36] have demonstrated that a malicious server can deceive the client model by manipulating the returned gradients to reconstruct its private data or implant backdoors. The existence of these attacks inspired our work: a trusted server can similarly leverage this channel to embed a watermark through benign gradient injection.

On the other hand, in response to attacks like FSHA, the research community has proposed corresponding gra-

dient anomaly detection methods as defenses. These defenses pose a direct challenge to the stealthiness of the Sigil scheme. SplitGuard [37] first explored the detection of FSHA’s anomalous gradients. Its core idea is to actively inject incorrect labels and then detect anomalies based on the gradient’s sensitivity to them. Subsequently, Pinocchio’s Nose [38] argued that SplitGuard’s active injection could degrade model performance, so it employed a passive detection method by exploiting the inherent differences in directional consistency of FSHA gradients. SplitOut [39] addressed the limitations of Pinocchio’s reliance on empirically chosen hyperparameters and proposed collecting normal gradients as a reference distribution by simulating training with a small amount of local data prior to training, followed by comparison during training.

These detection methods impose a stealthiness requirement on any method that modifies gradients, whether for malicious attacks or benign watermarking. We evaluate Sigil’s stealthiness against these detection methods in Section 5.3.

3. Problem Formulation

This section first formally defines the threat model and specifies the capabilities of each party. Then it outlines the core design objectives of Sigil.

3.1. Threat Model

Based on the motivation articulated in the Introduction, we define our threat model within the context of U-SFL. This model consists of a trusted server and one or more non-colluding but potentially malicious clients. We assume that the adversary actively participates in the training process and possesses substantial capabilities, including white-box access to its local model and full knowledge of the watermarking mechanism, as detailed below.

Defender Assumptions

Role. The defender is the server² in the U-SFL framework.

Goal. The server is the legitimate owner of the model. Its objective is to embed a robust and stealthy watermark into the client’s model.

Capabilities and Knowledge. The server possesses its server-side model and has access to the full activation and gradient streams. However, it *cannot* access the client’s local data, labels, or model parameters.

Adversary Assumptions

Role. The adversary consists of one or more non-colluding malicious clients in the U-SFL framework.

Goal. The adversary’s goal is to obtain a complete, watermark-free, high-performance model for illicit use and distribution. To achieve this, the adversary has two sub-goals: (1) Remove the watermark from their local client-side model; (2) Recover the server-side model. The threat model in this work focuses on countering the first sub-goal, where the malicious client attempts to eliminate the embedded watermark.

² strictly speaking the main server in U-SFL/SFL

Knowledge. We assume a strong adversary with the following knowledge and access privileges:

- **Scheme Knowledge:** The adversary fully understands the algorithmic mechanism of Sigil, but *does not* know the server’s secret watermark parameters $K = (M, b)$, where M denotes the embedding matrix and b denotes the watermark string.
- **Deployment Access:** The adversary has white-box access to their own client-side model, local data and labels, and the gradient/activation streams.

Capabilities. Given the above knowledge, the adversary can perform the following attacks:

- **Training-Time Noise Injection:** The adversary may attempt to disrupt the watermark embedding process by adding noise to the gradients during training.
- **Post-hoc Removal Attacks:** The adversary can apply various known watermark removal attacks—such as fine-tuning, pruning, and quantization—to their locally held watermarked model, attempting to remove the watermark without degrading main task performance.
- **Adaptive Subspace Removal Attack:** Leveraging its knowledge of the scheme, the adversary can collect and analyze gradients in real time to isolate the injected watermark information, and then perform targeted fine-tuning offline to remove the watermark.

3.2. Design Goals

Based on the threat model defined in Section 3.1, we establish the core design objectives for the Sigil scheme. The scheme must demonstrate fidelity, stealthiness, and robustness. Furthermore, it must support reliable embedding and verification, impose low computational and storage overhead, and provide sufficient capacity to uniquely identify ownership.

- **Fidelity:** Watermark embedding must have a negligible impact on the main task’s performance.
- **Stealthiness:** The watermarking mechanism must be statistically indistinguishable from a benign training process so that it can evade anomaly detection.
- **Robustness:** The watermark must resist various removal attacks defined in the adversary’s threat model, maintaining its effectiveness after the attack.

4. Method

This section describes the proposed Sigil framework, including design rationale, implementation details, and a geometric interpretation.

4.1. Design Rationale

We begin from the U-SFL workflow and the role-capability constraints. Although the server cannot access the

client's local data, labels, or model parameters, it observes the smashed activations uploaded by the client and controls the gradients returned to the client. Since the client's model update relies entirely on this gradient, it constitutes the only feasible channel for the server to influence the client's learning.

Motivated in part by SL attack techniques such as FSHA, we use the server-visible activation space as the embedding carrier and formulate the watermark as a predefined statistical constraint within this space, a watermark that is independent of both data and labels. During training, the server computes a watermark loss in parallel with the primary-task loss, combines the resulting watermark gradient with the task gradient, and returns the merged gradient to the client. This gradient-injection procedure embeds the watermark without altering the normal training workflow.

A malicious client, aware of the scheme's details, might try to use existing gradient detection methods (developed for FSHA) to detect anomalies caused by the watermark in the gradient. Furthermore, they might design an adaptive attack to analyze the gradient stream and attempt to estimate the watermark subspace for a targeted removal attack.

To counter the threats of gradient anomaly detection and adaptive attacks, we adaptively clip the norm of the watermark gradient relative to the task gradient. This adaptive clipping makes the statistical features of the watermark gradient difficult to distinguish from the normal gradient flow, enhancing the scheme's stealthiness. As a result, even if a malicious client knows the scheme's design, it cannot detect or separate the watermark gradient without impairing the optimization of the main task, thus enforcing mandatory embedding.

In summary, our core approach is: **using gradient injection as the embedding mechanism and the statistical properties of the activation layer as the embedding target, thereby realizing implicit and mandatory watermarking.**

4.2. The Sigil Watermarking Framework

presents the implementation of the Sigil framework, which comprises three core phases: watermark initialization, embedding, and verification. The notation used throughout these processes is summarized in Table 2.

Watermark Initialization. Before the training process begins, the server generates the secret parameter pair $K = (M, b)$ as its ownership credential, consisting of an embedding matrix M and a watermark string b .

The embedding matrix M is an $\mathbb{R}^{d \times k}$ matrix with elements sampled independent and identically distributed (IID) from a standard normal distribution $\mathcal{N}(0, 1)$. As a Gaussian matrix, M is full-rank with high probability, which ensures the randomness and stability of the watermark subspace. It serves to project the high-dimensional activation A_{flat} into a fixed, k -dimensional watermark space.

The watermark string b is a secret bit string of length k , sampled uniformly at random from $\{0, 1\}^k$. This binary

TABLE 2. SUMMARY OF NOTATION.

Symbol	Description
t	Global communication round.
i	Client index.
$f_{c,i}^{(t)}, \theta_{c,i}^{(t)}$	Client-side model and its parameters at round t .
$f_{s,i}^{(t)}, \theta_{s,i}^{(t)}$	Server-side model and its parameters at round t .
f'_c, θ'_c	Suspicious client-side model for verification.
X_i, y_i	A batch of input data and private labels for client i .
$A_i^{(t)}, A_{\text{flat},i}^{(t)}$	Smashed data (activation) from client i and its flattened form, respectively.
$S_i^{(t)}$	Server's intermediate output sent back to client i .
$G_{\text{initial},i}^{(t)}$	Initial gradient ($\partial \mathcal{L}_{\text{main}} / \partial S_i^{(t)}$) sent from client i .
M, b	Watermark projection matrix and target bits.
k	The bit-length of the watermark.
$\mathcal{L}_{\text{main}}$	Main task loss function (e.g., Cross-Entropy).
\mathcal{L}_{wm}	Watermark loss function (BCE).
$G_{\text{main},i}^{(t)}$	Gradient of $\mathcal{L}_{\text{main}}$ w.r.t. client activation $A_i^{(t)}$.
$G_{\text{wm},i}^{(t)}$	Gradient of \mathcal{L}_{wm} w.r.t. client activation $A_i^{(t)}$.
$G'_{\text{wm},i}^{(t)}$	Watermark gradient after adaptive clipping.
$G_{\text{final},i}^{(t)}$	The final (composite) gradient sent to client i .
λ	Watermark strength (scaling ratio) for adaptive gradient clipping.
E	Number of local epochs for client training.

representation can directly encode information and is well-suited for the subsequent Binary Cross-Entropy (BCE) loss function.

Watermark Embedding via Gradient Injection. The watermark embedding process is seamlessly integrated into the standard U-SFL workflow. All watermark-related operations are performed solely on the server side and remain entirely transparent to the client.

Sigil leverages these secret parameters (M, b) to define the watermark as a statistical constraint on the server-visible activation space. Specifically, through gradient injection, Sigil forces the client's model to generate activations (A_{flat}) that statistically match the target bit string b when projected by M . The injected gradient is therefore formulated to minimize this projection difference.

A key challenge in this process is maintaining stealthiness. Simply adding the raw watermark gradient G_{wm} to the main task gradient G_{main} presents a stealthiness problem [38], [39]. In the early stages of training, before the watermark is well embedded, the watermark loss is often much larger than the main task loss, causing the norm of G_{wm} to be abnormally large. This would make the statistical features (like the norm) of the final gradient deviate significantly from the normal distribution, creating a detectable anomaly signal for a malicious client. Moreover, this dominance would allow a malicious client to separate and extract key watermark information (e.g., the gradient's subspace) by analyzing gradient differences, facilitating targeted watermark removal attacks, as we demonstrate in Section 5.4.

To address the challenge, we employ an adaptive norm clipping strategy that directly regulates the gradient magnitude instead of reweighting the losses. This method dynam-

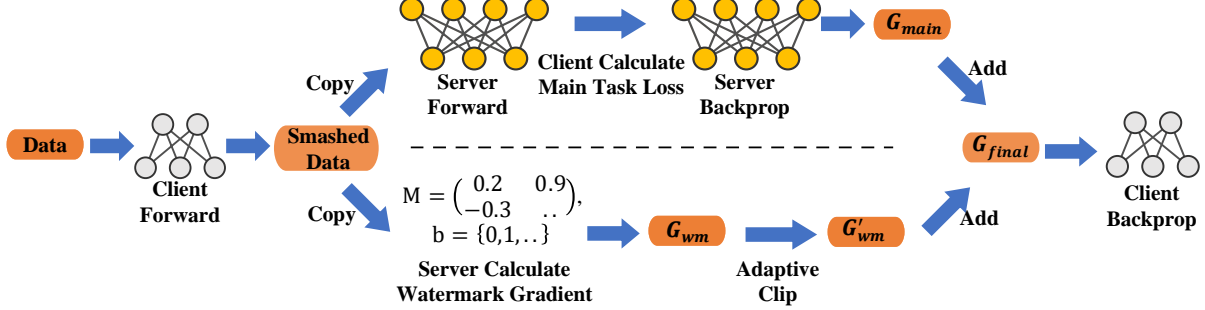


Figure 2. The Sigil Watermark Embedding while U-SFL Training.

ically links the upper bound of the watermark gradient's norm to the main task gradient's norm, controlled by a hyperparameter λ , yielding a clipped gradient G'_{wm} .

Finally, the server produces a composite gradient G_{final} and sends it back to client i . From the client's perspective, $G_{final}^{(i,t)}$ is statistically indistinguishable from a standard gradient. Without access to the clean reference gradient, the client cannot detect the subtle watermark perturbations. Therefore, the client is compelled to apply them, thereby being forced to embed the watermark.

Algorithm 1 and Figure 2 illustrate how Sigil performs watermark embedding within a complete U-SFL forward and backpropagation pass. For clarity, these illustrations focus on the core embedding logic of a single pass, omitting the details of multiple training rounds and the final model aggregation on both sides.

The process begins when the client performs its local forward pass and sends its activation $A_i^{(t)}$ to the server (Line 2). Upon receiving this activation, the server proceeds along two parallel branches: the main task computation (upper branch in Figure 2) and the watermark task computation (lower branch).

For the main task, the server follows the standard U-SFL protocol: it completes the forward pass, returns the logits $S_i^{(t)}$ to the client (Line 4), and subsequently receives the initial gradient $G_{initial,i}^{(t)}$ (Line 6). The server then uses this gradient to perform backpropagation, updating its server-side model and calculating the main task's gradient with respect to the client's activation, $G_{main}^{(i,t)}$ (Lines 7-8).

In parallel, for the watermark task, the server uses its secret parameters $K = (M, b)$ to compute the watermark loss \mathcal{L}_{wm} . This loss is defined as the BCE between the target watermark string b and the predicted bit string:

$$\mathcal{L}_{wm} = \text{BCE}(\text{sigmoid}(A_{flat}^{(i,t)} \cdot M), b). \quad (1)$$

Based on this loss, the server calculates the corresponding raw watermark gradient $G_{wm}^{(i,t)}$ (Line 9). The server then applies the adaptive norm clipping mechanism (Line 10) to generate the stealthy, clipped gradient $G'_{wm}^{(i,t)}$:

$$G'_{wm}^{(i,t)} = \min \left(1, \lambda \cdot \frac{\|G_{wm}^{(i,t)}\|_2}{\|G_{wm}^{(i,t)}\|_2 + \epsilon} \right) \cdot G_{wm}^{(i,t)}, \quad (2)$$

Algorithm 1 U-SFL Training with Sigil Embedding (Single Batch Step within Round t)

Input: Client i 's data batch (X_i, y_i) and current model $\theta_{c,i}^{(t)}$; Server's current model $\theta_{s,i}^{(t)}$, watermark parameters (M, b) and λ .
Output: Locally updated client model $\theta_{c,i}^{(t)}$ and server model $\theta_{s,i}^{(t)}$.

Client i Executes:

- 1: $A_i^{(t)} \leftarrow f_{c,i}^{(t)}(X_i)$
- 2: Send $A_i^{(t)}$ to Server

Server Executes:

- 3: $S_i^{(t)} \leftarrow f_{s,i}^{(t)}(A_i^{(t)})$
- 4: Send $S_i^{(t)}$ back to Client i

Client i Executes:

- 5: $G_{initial,i}^{(t)} \leftarrow \frac{\partial \mathcal{L}_{main}(S_i^{(t)}, y_i)}{\partial S_i^{(t)}}$
- 6: Send $G_{initial,i}^{(t)}$ to Server

Server Executes:

- 7: $\theta_{s,i}^{(t+1)} \leftarrow \text{Update}(\theta_{s,i}^{(t)}, G_{initial,i}^{(t)})$
- 8: $G_{main,i}^{(t)} \leftarrow \text{Backprop}(G_{initial,i}^{(t)}, A_i^{(t)})$
- 9: $G_{wm,i}^{(t)} \leftarrow \frac{\partial \mathcal{L}_{wm}(A_i^{(t)}, M, b)}{\partial A_i^{(t)}}$
- 10: $G'_{wm,i}^{(t)} \leftarrow \min(1, \lambda \cdot \frac{\|G_{wm,i}^{(t)}\|_2}{\|G_{wm,i}^{(t)}\|_2 + \epsilon}) \cdot G_{wm,i}^{(t)}$
- 11: $G_{final,i}^{(t)} \leftarrow G_{main,i}^{(t)} + G'_{wm,i}^{(t)}$
- 12: Send final gradient $G_{final,i}^{(t)}$ to Client i

Client i Executes:

- 13: $\theta_{c,i}^{(t+1)} \leftarrow \text{Update}(\theta_{c,i}^{(t)}, G_{final,i}^{(t)})$

where ϵ is a small constant to avoid division by zero. Finally, the server combines the gradients from both the main task and the watermark task (Line 11) to obtain the composite gradient $G_{final}^{(i,t)}$:

$$G_{final}^{(i,t)} = G_{main}^{(i,t)} + G'_{wm}^{(i,t)}. \quad (3)$$

This final gradient is then sent to the client (Line 12), which uses it to perform local backpropagation and update the client-side model.

Watermark Verification. The watermark verification process allows the owner to confirm ownership of a potentially leaked model. A key advantage of this verification method is its data-agnostic nature: the verifier does not need access to any private original training data.

The verification process assumes white-box access to the target model f'_c , specifically the ability to perform a forward pass and obtain the activation output A' at the split point. Using these activations and the secret watermark parameters $K = (M, b)$, the verifier checks whether the embedded statistical constraint is preserved.

We quantify the verification result using the Watermark Success Rate (WSR). Ownership is confirmed if the computed WSR exceeds a preset threshold τ . This statistically justified threshold is determined empirically, as described in Section 5.1.

The specific procedure outlined in Algorithm 2 is as follows:

The verifier first generates a set of N random input tensors X_{rand} , (e.g., from $\mathcal{N}(0, 1)$) (Line 1). It then performs a forward pass on the suspect model to get the activations A' (Line 2), flattens them (Line 3), and projects them using the secret matrix M to get the predicted probabilities \hat{b} (Line 4). These probabilities are subsequently rounded to extract the predicted bit string B' (Line 5).

Finally, the WSR_{verify} is calculated (Line 6) by comparing the predicted bit string B' against the target watermark b , aggregated across all samples and bits:

$$WSR = \frac{\sum_{i=1}^N \sum_{j=1}^k \mathbb{I}(b'_{ij} == b_j)}{N \times k}. \quad (4)$$

Here, N is the number of random samples used for verification, k is the watermark length (defined in Table 2), b'_{ij} is the predicted j -th bit for the i -th sample, and b_j is the j -th bit of the target watermark. $\mathbb{I}(\cdot)$ is the indicator function. This calculated WSR is then compared to the threshold τ to return the final boolean verification result (Lines 7-11).

Geometric Interpretation of the Embedding Mechanism. This section provides a geometric interpretation of the Sigil framework’s embedding process that explains its effectiveness and high fidelity, aligning with two key experimental observations. We model the gradient updates as occurring in two distinct subspaces. The first is the watermark subspace (S_{wm}), a fixed k -dimensional subspace spanned by the column vectors of the secret matrix M . The second is the main task subspace (S_{main}), which is a low-dimensional subspace in a statistical sense and determined by the data distribution and the main task loss.

Since S_{wm} is generated through the random initialization of M , and S_{main} is determined by the data’s semantics, the two subspaces are statistically independent. A key property of high-dimensional geometry is that two independent high-dimensional subspaces are almost always nearly orthogonal. This can be supported by a more fundamental quantitative result [40]: in a high-dimensional space \mathbb{R}^d , the expected squared dot product (i.e., $\cos^2(\theta)$) between two independently and randomly chosen unit vectors is:

Algorithm 2 Sigil Post-hoc Data-Free Verification

Verifier Executes:

Input: Suspect model parameters θ'_c ; Watermark parameters (M, b) ; Threshold τ

Output: A boolean value indicating whether passing the ownership verification process.

```

1: Generate a set of  $N$  random tensors  $X_{\text{rand}}$  (e.g., from  $\mathcal{N}(0, 1)$ )
2:  $A' \leftarrow f_c(X_{\text{rand}}, \theta'_c)$ 
3:  $A'_{\text{flat}} \leftarrow \text{Flatten}(A')$ 
4:  $\hat{b} \leftarrow \text{sigmoid}(A'_{\text{flat}} \cdot M)$ 
5:  $B' \leftarrow \text{round}(\hat{b})$ 
6:  $WSR_{\text{verify}} \leftarrow \frac{\sum_{i=1}^N \sum_{j=1}^k \mathbb{I}(B'_{ij} == b_j)}{N \times k}$ 
7: if  $WSR_{\text{verify}} > \tau$  then
8:   return True
9: else
10:  return False
11: end if

```

$$E[\cos^2(\theta)] = \text{Var}(\cos(\theta)) = \frac{1}{d}. \quad (5)$$

This near-orthogonality directly underpins Sigil’s high fidelity. It implies that the watermark gradient G'_{wm} is a small, non-interfering perturbation to the main task’s optimization. We quantitatively confirm this in our experiments in Section 5.2: the cosine similarity between the main task gradient G_{main} and the watermark gradient G_{wm} consistently remains on the order of 10^{-4} .

Orthogonality also explains why Sigil remains effective even under very small watermark strengths (small λ). Within the S_{wm} subspace, the watermark gradient G'_{wm} provides a persistent, biased signal that always points toward the watermark target. In contrast, the projection of the main task gradient G_{main} onto this subspace is an unbiased random noise with a zero mean. Over long-term training, this persistent, biased signal continuously influences the model’s projections within the watermark subspace, causing a drift that manifests as the model learns the watermark. This aligns with our experimental observation in Section 5.2 that the watermark can still be successfully embedded ($WSR > 99\%$) even at $\lambda = 0.01$.

However, this geometric orthogonality between S_{main} and S_{wm} and the persistent bias of G'_{wm} also implies theoretical separability of the watermark signal, making the adaptive subspace removal attack in Section 5.4 theoretically viable. Our adaptive gradient clipping mechanism is precisely designed to counter this by attenuating the strength of the watermark gradient, causing it to be statistically masked by other signals in G_{final} . This reduces the accuracy of such separation, thereby enhances the scheme’s stealthiness and robustness against this specific adaptive attack.

5. Evaluation

This section provides a comprehensive evaluation of the proposed Sigil watermarking framework in terms of fidelity,

stealthiness, robustness, and key design choices, including the split strategy and watermark length.

5.1. Experiment Setup

Datasets, Models, and Settings. We evaluate Sigil on two benchmark datasets: CIFAR-10 (using ResNet-18 and VGG11) and Tiny-ImageNet (using MobileNetV2 and DenseNet-121). We simulate a 10-client IID U-SFL setting. Unless otherwise specified, our default configuration uses ResNet-18 on CIFAR-10 with the split point placed after the third residual block. The watermark strength is set to $\lambda = 0.1$ and the watermark length to $k = 50$. Additional implementation details, including full hyperparameters and split points for other models, are provided in Appendices A and B.

Evaluation Metrics. We use Top-1 Accuracy (Acc) to measure main-task performance and WSR (defined in Eq. 4) to assess watermark effectiveness. To establish a statistically significant verification threshold τ , we adapt the methodology of Lukas *et al.* [33]. Specifically, we empirically evaluate our ResNet-18 baseline by testing 100 randomly generated watermark parameters against 30 independently trained clean models, and observe that the resulting WSR values follow a normal distribution. From this distribution, we determine that a 5-sigma significance level (p -value $< 3 \times 10^{-7}$) corresponds to a WSR of 68%. Accordingly, we conservatively set the verification threshold to $\tau = 70\%$, exceeding the 5-sigma level and providing strong statistical confidence for all subsequent claims.

5.2. Fidelity

This section evaluates the fidelity of Sigil by comparing a clean model (trained without watermarking) with watermarked models (WM) under different watermark strengths (λ). Figure 3 illustrates the training dynamics of Sigil. Across all four task settings, the accuracy of the watermarked models nearly coincides with that of the clean baseline, indicating high fidelity. Table 3 presents detailed results supporting this observation. The accuracy difference between the watermarked models and the clean baseline remains within a narrow range of $\pm 0.6\%$ for all tasks. Furthermore, accuracy does not exhibit a noticeable downward trend as λ increases, suggesting that watermark strength has no significant negative impact on main-task performance.

Notably, the watermark embedding process is highly effective. Even at an extremely low strength of $\lambda = 0.01$, the WSR consistently reaches 99% or higher, far exceeding the verification threshold of $\tau = 70\%$. This demonstrates that Sigil remains effective even under low gradient strength, which aligns with the geometric analysis in Section 4.3.

The geometric orthogonality further provides a strong theoretical foundation for this high fidelity. As shown in Table 3, the average cosine similarity between G_{wm} and G_{main} remains extremely small (ranging from 1×10^{-4} to

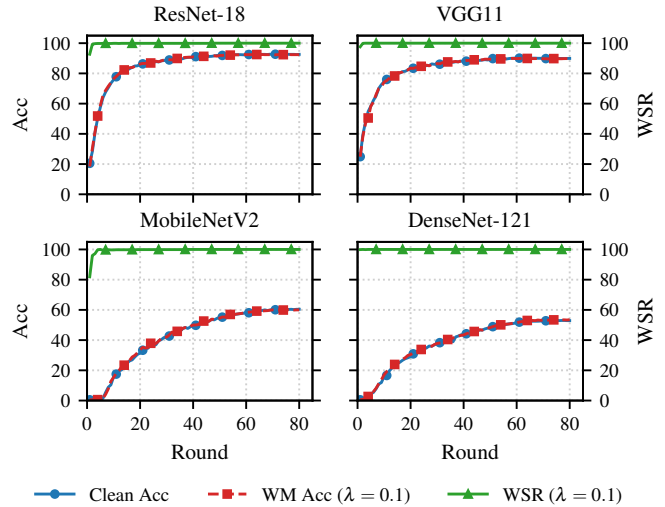


Figure 3. Fidelity and Effectiveness Evaluation on All Tasks.

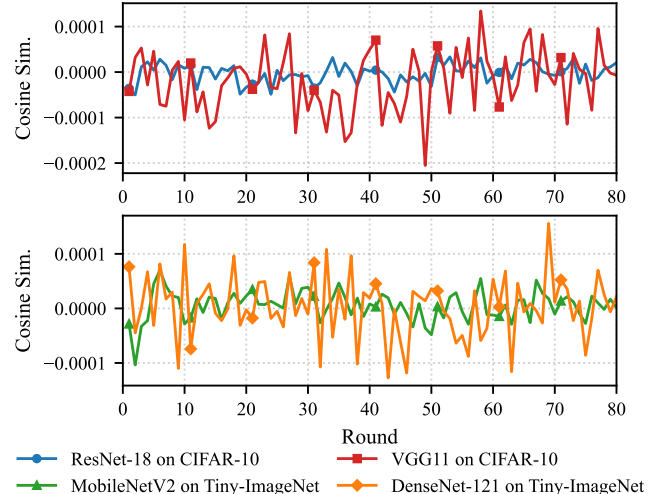


Figure 4. Gradient Orthogonality Analysis (Cosine Similarity).

1×10^{-6}). Figure 4 illustrates that this similarity remains stably centered around zero (with absolute values $< 1 \times 10^{-4}$) throughout training. This confirms that the two gradients are statistically orthogonal, enabling the watermark to be embedded as a non-interfering signal with negligible impact on the main task.

5.3. Stealthiness

This section evaluates the stealthiness of Sigil by comparing the gradient streams of the clean baseline and the watermarked models against two state-of-the-art anomaly detection frameworks: Gradient Scrutinizer [38] and SplitOut [39].

Gradient Scrutinizer. Gradient Scrutinizer monitors the distribution of gradient cosine similarities (Figure 5, subplots 1–3), where greater separation between same-label and

TABLE 3. QUANTITATIVE RESULTS FOR FIDELITY, EFFECTIVENESS, AND GRADIENT ORTHOGONALITY. EACH CELL SHOWS TOP: MAIN TASK ACC (%) / MIDDLE: WSR (%) / BOTTOM: MEAN COSINE SIMILARITY.

Model / Dataset	Baseline (Clean)	Sigil Watermark (λ value)		
		$\lambda = 0.01$	$\lambda = 0.1$	$\lambda = 1.0$
ResNet-18 / CIFAR-10	92.6%	92.4%(-0.2)	92.4%(-0.2)	92.8%(+0.2)
	-	99.1%	100%	100%
	-	2.5e-6	-2.1e-6	1.6e-6
VGG11 / CIFAR-10	89.9%	89.9%	89.7%(-0.2)	89.9%
	-	99.9%	100%	100%
	-	-1.1e-4	-2.0e-5	-1.9e-5
MobileNetV2 / Tiny-ImageNet	60.4%	60.5%(+0.1)	60.0%(-0.4)	60.1%(-0.3)
	-	99.2%	100%	100%
	-	-1.8e-5	5.5e-6	7.3e-6
DenseNet-121 / Tiny-ImageNet	52.9%	53.2%(+0.3)	53.5%(+0.6)	52.9%
	-	100%	100%	100%
	-	-2.4e-6	3.6e-6	-7.7e-6

different-label inputs represents more normal behavior. It then aggregates these observations into a normality score (subplot 4), where scores below 0.5 indicate an anomaly.

As shown in Figure 5, the similarity distributions of the clean model and the WM model with $\lambda = 0.1$ are highly consistent. In contrast, the WM model with $\lambda = 1.0$ exhibits some anomalous fluctuations during the early stages of training, though it stabilizes later as the watermark becomes embedded and its gradient influence diminishes. As reflected in the final normality score, both the clean baseline and the $\lambda = 0.1$ watermarked model maintain a perfect score of 1.0, while the $\lambda = 0.1$ watermarked model briefly dips before recovering. This indicates that although Gradient Scrutinizer can detect the stronger gradients produced under $\lambda = 1.0$, our gradient clipping mechanism ensures that the $\lambda = 0.1$ gradients remain statistically indistinguishable from those of the clean model, thereby meeting the stealthiness requirement.³

SplitOut. SplitOut first constructs a normal gradient distribution through local simulation, and then counts, for each training round, the number of gradients that deviate from this distribution (i.e., outliers). It flags an anomaly when this count exceeds a preset threshold (e.g., half of a batch).

As shown in Figure 6, the clean model naturally exhibits a noise baseline of approximately 5–15 outliers. The outlier count for WM ($\lambda = 1.0$) is consistently higher than this clean baseline. In contrast, the outlier curves for WM ($\lambda = 0.1$) and WM ($\lambda = 0.01$) remain tightly aligned with the clean baseline’s fluctuation range. Even the peak outlier count for WM ($\lambda = 1.0$) (around 40) remains far below the typical batch-level detection threshold (128 for our batch size of 256).

3. We observed that reproducing the detection logic of Gradient Scrutinizer is highly sensitive to the split point in our U-SFL setup. We were unable to replicate its intended behavior at our default split point (Layer 3), as it produced anomalous outputs even for clean models. However, we successfully reproduced its expected behavior at the Layer 4 split. Accordingly, all results in Figure 5 are based on the Layer 4 split to ensure valid and fair comparisons.

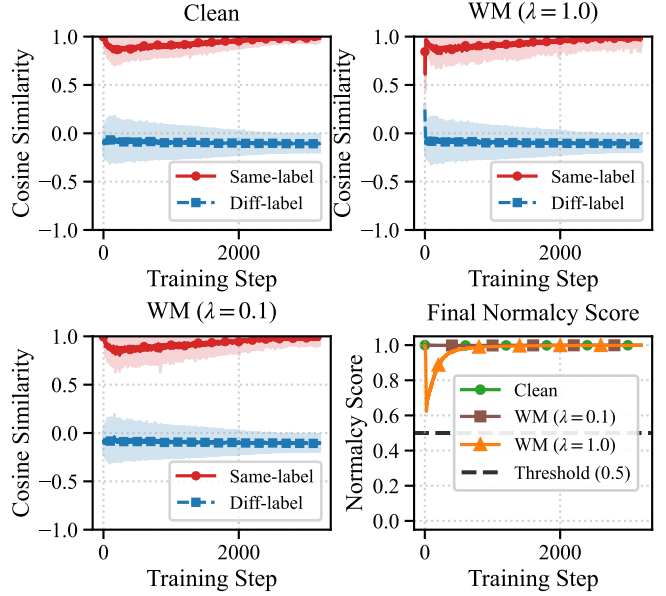


Figure 5. Stealthiness Evaluation against Gradient Scrutinizer

Aggregating the results from both state-of-the-art detectors, we confirm the high stealthiness of the Sigil framework. The experiments clearly demonstrate that watermark strength λ is the dominant factor: when λ is large (e.g., 1.0), the watermark introduces detectable statistical deviations, whereas smaller values (e.g., 0.1) allow Sigil to effectively suppress its gradient impact and evade detection. Combined with the findings in Section 5.2, Sigil’s ability to remain highly effective even at extremely low strengths (e.g., $\lambda = 0.01$) indicates that the practical feasible range for λ is wide, underscoring the scheme’s utility.

5.4. Robustness

This section evaluates the robustness of Sigil against the three attack capabilities defined in our threat model.

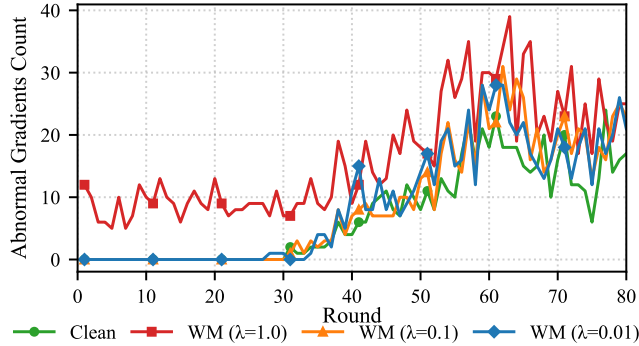


Figure 6. Stealthiness Evaluation against SplitOut

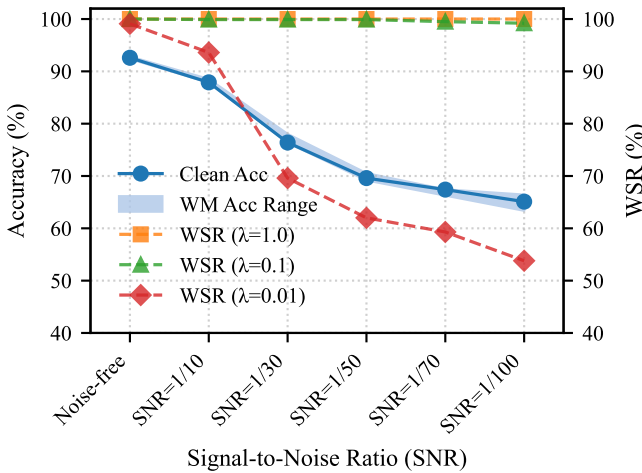


Figure 7. Robustness against Training-Time Noise Injection (SNR).

Robustness Against Training-Time Noise Injection. To simulate a client interfering with the G_{final} transmission, we adopt ideas from prior works [41], [42] to inject Gaussian noise, quantified using the Signal-to-Noise Ratio (SNR). As shown in Figure 7, we plot results across decreasing SNR values (i.e., increasing noise) from “Noise-free” to $1/100$, where lower SNR corresponds to stronger noise.

As shown in Figure 7, the accuracy of both the clean model and the watermarked models steadily decreases as noise strength increases (i.e., as SNR decreases). Accuracy drops from approximately 90% to 70% as SNR decreases from noise-free to $1/50$, and further declines to around 65% at $1/100$.

In contrast, the Sigil watermark exhibits strong robustness to gradient noise. The WSR for $\lambda = 1.0$ remains at 100% even under the highest noise level ($\text{SNR} = 1/100$), while the WSR for $\lambda = 0.1$ remains at 99.2% under the same conditions. The $\lambda = 0.01$ watermark is more affected, dropping to 69.6% (below the verification threshold $\tau = 70\%$) at $\text{SNR} = 1/30$. However, at this point, the main-task accuracy has already decreased by over 15%, meaning the attacker cannot obtain a high-performance clean model. Therefore, this attack is considered unsuccessful.

Robustness Against Post-hoc Removal Attacks. We evaluate Sigil against fine-tuning, pruning, and quantization, comparing it to simulated backdoor (BDWM) and parameter (PWM) watermark baselines [20], [26].

The results are presented in Table 4. PWM exhibits extremely high robustness ($\text{WSR} \geq 98.0\%$) across all attacks due to its inherent mechanism. In contrast, BDWM is more fragile, with its WSR decreasing to 95.6% under fine-tuning and failing completely under 80% pruning.

Sigil demonstrates excellent robustness to both fine-tuning and quantization. Under 100 steps of strong fine-tuning and extreme INT4 quantization, the WSR for all Sigil configurations remains virtually unaffected ($\text{WSR} \geq 99.0\%$ for $\lambda = 0.01$), matching the performance of the most robust PWM baseline. For pruning, Sigil also maintains high robustness: at an 80% pruning rate, the WSR for $\lambda = 1.0$ drops only slightly to 97.9%, while $\lambda = 0.1$ drops to 94.6%. The weakest $\lambda = 0.01$ model experiences the largest reduction to 87.5%, yet this remains well above the verification threshold of 70%. Overall, these experiments confirm that Sigil is highly resilient against these three common post-hoc removal attacks.

Robustness Against Adaptive Subspace Removal Attack. We further design a targeted adaptive removal attack to evaluate the robustness of Sigil and the effect of gradient clipping, leveraging full knowledge of the Sigil scheme in accordance with our malicious client threat model.

Under this threat model, we assume that the adversary possesses two key pieces of knowledge:

Knowledge 1: The adversary understands that the watermark gradient signal is stronger during the early training phase (e.g., $R_{\text{early}} \in [0, 10]$ rounds), whereas the gradient becomes dominated by the main task in the later phase (e.g., $R_{\text{late}} \in [70, 80]$ rounds) after the watermark has been embedded. (A visualization of the gradient components over training is provided in Appendix C.)

Knowledge 2: The adversary is aware of a derivable mathematical property: the watermark gradient G_{wm} , the activation pattern A_{flat} , and the projection matrix M all lie within the same low-dimensional watermark subspace. Intuitively, because the watermark loss $\mathcal{L}_{\text{wm}} = \text{BCE}(\text{sigmoid}(A_{\text{flat}} \cdot M), b)$ (see Eq. 1) is computed directly from the projection of A_{flat} onto M , its gradient $G_{\text{wm}} = \frac{\partial \mathcal{L}_{\text{wm}}}{\partial A_{\text{flat}}}$ is, by the chain rule, linearly related to the column vectors of M that define this subspace. (A detailed mathematical derivation is provided in Appendix D.)

Based on these insights, the adversary constructs the following adaptive attack:

1. Online Gradient Collection: The malicious client collects all $G_{\text{final}}^{(i,t)}$ gradients from two phases: the early phase ($R_{\text{early}} \in [0, 10]$), which is assumed to be watermark-dominated, and the late phase ($R_{\text{late}} \in [70, 80]$), which is assumed to be dominated by the main task.

2. Offline Analysis and Subspace Estimation:

- The attacker performs PCA on the late-phase gradient set G_{late} and extracts the top N principal components as the main-task gradient subspace V_{main} .

TABLE 4. ROBUSTNESS AGAINST POST-TRAINING REMOVAL ATTACKS (RESNET-18/CIFAR-10). EACH CELL SHOWS TOP: ACC (%) / BOTTOM: WSR (%).

Attack Type	Strength	Clean (Acc)	Baselines (Sim.)		Sigil (λ value)		
			BDWM	PWM	$\lambda = 1.0$	$\lambda = 0.1$	$\lambda = 0.01$
No Attack	(None)	92.6%	92.1% 99.9%	92.4% 100%	92.8% 100%	92.4% 100%	92.4% 99.1%
Fine-tuning	50 steps	91.5%	91.4% 98.1%(-1.8)	91.6% 100%	91.8% 100%	91.8% 100%	91.4% 99.0%(-0.1)
	100 steps	91.3%	91.3% 95.6%(-4.3)	91.5% 100%	91.6% 100%	91.5% 100%	91.2% 99.0%(-0.1)
	Ratio 60%	52.0%	65.9% 75.8%(-24.1)	60.3% 100%	48.2% 100%	53.7% 99.7%(-0.3)	53.6% 98.3%(-1.6)
Pruning	Ratio 80%	14.8%	10.5% 0%(-99.9)	11.7% 100%	11.7% 97.9%(-2.1)	10.5% 94.6%(-5.4)	10.0% 87.5%(-12.4)
	FP16	92.6%	92.2% 99.9%	92.4% 100%	92.8% 100%	92.4% 100%	92.4% 99.1%
	INT8	92.6%	92.2% 99.9%	92.4% 100%	92.8% 100%	92.4% 100%	92.4% 99.1%
Quantization	INT4	89.6%	90.4% 99.8%(-0.1)	90.2% 98.0%(-2)	91.1% 100%	91.4% 100%	90.5% 99.0%(-0.1)

- The attacker projects the early-phase gradients G_{early} onto the orthogonal complement of V_{main} , obtaining the residual gradients G_{residual} .
- The attacker applies PCA on G_{residual} and extracts the top k' principal components, treating this as the estimated watermark gradient subspace V_{wm} .

3. Targeted Fine-tuning: The attacker fine-tunes the model using a new composite loss $\mathcal{L}_{\text{total}} = \mathcal{L}_{\text{main_task}} + \gamma \cdot \mathcal{L}_{\text{attack}}$. Here, $\mathcal{L}_{\text{attack}}$ is an orthogonality-based penalty that suppresses the projection of activations A_{flat} onto the estimated watermark subspace V_{wm} . Letting w_j denote the PCA variance of component v_j , the penalty is defined as $\mathcal{L}_{\text{attack}}(A) = \sum_{j=1}^{k'} w_j \cdot (A_{\text{flat}} \cdot v_j)^2$.

The subspace V_{wm} identified in Step 2 represents the adversary's approximation of the watermark subspace. In Step 3, the orthogonality penalty constrains the activations A_{flat} to avoid this estimated subspace, thereby attempting to remove the watermark.

We evaluated Sigil models with varying watermark strengths λ under this adaptive attack, modifying the early-phase range R_{early} (e.g., first 10, 5, 2, or 1 rounds). The late-phase range was fixed at $R_{\text{late}} \in [70, 80]$, with $k' = 64$, $\gamma = 1$, and fine-tuning performed for 100 epochs using a learning rate of 1×10^{-4} .

Results are shown in Table 5. When λ is high ($\lambda = 1.0$), the G_{wm} signal is too strong in the early phase. The adversary can relatively accurately separate the subspace V_{wm} in all four R_{wm} settings, causing the WSR to drop to $\approx 60\%$ (below the $\tau = 70\%$ threshold) post-attack. Meanwhile, the main task accuracy is maintained at $\approx 89\%$, indicating the adaptive attack successfully removed the watermark while preserving utility.

When $\lambda = 0.1$, the watermark gradient norm is clipped to 10% of the main task gradient, reducing its strength in early rounds and making it harder to analyze. The WSR

remains $\approx 99\%$ for $R_{\text{wm}} = 10$ and 5, showing the watermark signal was masked by noise and other gradients. For $R_{\text{wm}} = 2$ and 1, the WSR drops to 80% and 86%, respectively. Although these reductions reflect some impact from the attack, both values remain above the 70% threshold. At $\lambda = 0.01$, the watermark is too weak to analyze, causing the attacker's subspace estimation to fail. Consequently, the WSR stays at 97–99%. Overall, these results indicate that the adaptive gradient clipping effectively defends against this attack.

Summary of Robustness. Aggregating the results from training-time noise injection, post-hoc removal attacks, and adaptive subspace removal attacks, we find that the trade-off parameter λ also directly governs Sigil's robustness. In the noise and pruning experiments, $\lambda = 0.01$ was slightly less robust than $\lambda = 0.1$. However, against the adaptive attack, $\lambda = 0.01$ was more robust than $\lambda = 0.1$ precisely because it was stealthier and harder to analyze. This re-confirms λ as Sigil's core hyperparameter, providing an adjustable balance between stealthiness and robustness. In all cases, both $\lambda = 0.1$ and $\lambda = 0.01$ successfully maintained the watermark against attacks, balancing effectiveness, stealthiness, and robustness.

5.5. Ablation Studies

This section conducts ablation studies on the split point and the length of watermark. Other factors, such as client count and Non-IID data distribution, are discussed in Appendix E.

Ablation on Split Strategy. As shown in Table 6, in the No Attack column, the Acc for all split points stable within the 92.1%–92.4% range, and the WSR reaches 99.8% or higher.

TABLE 5. ROBUSTNESS AGAINST THE ADAPTIVE SUBSPACE REMOVAL ATTACK. EACH CELL SHOWS TOP: ACC (%) / BOTTOM: WSR (%).

Watermark Strength (λ)	Before Attack	Adaptive Attack (using R_{wm} rounds)			
		$R_{wm}=10$	$R_{wm}=5$	$R_{wm}=2$	$R_{wm}=1$
$\lambda = 1.0$	92.8%	87.6%	89.2%	88.2%	89.8%
	100%	60.5%(-39.5)	61.1%(-38.9)	58.0%(-42.0)	59.3%(-40.7)
$\lambda = 0.1$	92.4%	87.9%	88.1%	88.2%	88.7%
	100%	99.7%(-0.3)	99.6%(-0.4)	79.7%(-20.3)	86.1%(-13.9)
$\lambda = 0.01$	92.4%	87.1%	88.8%	88.9%	88.7%
	99.1%	98.0%(-1.1)	97.2%(-1.9)	98.9%(-0.2)	98.8%(-0.3)

This indicates that Sigil can be flexibly deployed at different depths of the model without impacting its baseline fidelity and effectiveness.

Stealthiness improves significantly at deeper split points. The SplitOut outlier count, while fluctuating in shallow layers (16.7 for Layer 1 and 20.44 for Layer 2), drops substantially to 8.95 (Layer 3) and 0 (Layer 4). This trend is broadly consistent for robustness. Under extreme noise interference ($SNR = 1/100$), the WSR surges from 73.7% (Layer 1) to 99.5% (Layer 4). Similarly, under 80% pruning, the WSR at Layers 2-4 ($\geq 94.6\%$) is markedly superior to Layer 1 (88.6%).

As shown in Table 6, we also evaluated the adaptive subspace removal attack, finding that while all split points remain robust ($WSR > 70\%$), the most effective analysis window(i.e., the optimal R_{wm} rounds) changes with depth. Shallow layers (Layer 1, 2) were most vulnerable to analysis of the first 5/10 rounds ($R_{wm} = 5/10$), while the middle layer (Layer 3) was only vulnerable at the very beginning ($R_{wm} = 1/2$), and the deep layer (Layer 4) was similarly impacted ($WSR \approx 80\%$), but remained robust above the 70% threshold. We hypothesize this is because deeper activation layers encode higher-level, more stable semantic features, which alters the statistical properties and embedding dynamics of the watermark signal.

In summary, the results show that embedding at deeper locations significantly improves stealthiness and robustness. However, deeper split points also impose a higher computational overhead on the client. Our choice of Layer 3 as the baseline is a comprehensive trade-off between robustness, stealthiness, and computational cost.

Ablation on Watermark Length. We conduct this ablation at the default split point (Layer 3), where the activation tensor has a total dimension of 16,384, providing a theoretical reference for capacity.

As shown in Table 7, Sigil demonstrates significant watermark capacity. In the No Attack column, the WSR remains at 100% even as the watermark length k increases to 3,000. However, this high capacity comes at the cost of other key attributes. As k increases, the Acc slightly drops from 92.4% to 91.7%. And as we increased k further to 4000, the Acc collapsed completely, defining the ultimate fidelity boundary for this task. Robustness against standard attacks also declines: under 80% pruning, WSR falls from 94.6% ($k = 50$) to the 84.8%-88.5% range ($k \geq 500$).

The most severe cost of increasing k is to stealthiness. As shown in the table’s SplitOut column, the average outlier count surges from 8.95 ($k = 50$) to 592.39 ($k = 3000$). This makes high-capacity Sigil statistically trivial to detect, failing the stealthiness requirement.

Against the adaptive subspace removal attack, the watermark’s robustness shows a complex, non-monotonic trend. As shown in Table 7, the model remains robust at $k = 50$. At intermediate capacities, the attack becomes viable: $k=500$ is vulnerable to analysis of the first 10 rounds ($R_{wm} = 10$), and $k=1000$ is vulnerable to analysis of the first 5 rounds ($R_{wm} = 5$). Counter-intuitively, the model’s robustness is restored at $k = 2000/3000$. We also observe that the optimal analysis window for the attack shifts progressively earlier as k increases.

This result validates the effectiveness of our adaptive gradient clipping mechanism. Although a larger k generates a much larger raw watermark gradient, our clipping formula (Eq. 2) strictly caps its norm to the same threshold. We hypothesize this complex “dip-and-rise” robustness trend is related to the high-dimensional optimization dynamics involving the orthogonality of the S_{wm} and S_{main} subspaces and the changing dimensionality k , which remains an open question.

Watermark length k is a critical design choice. While our baseline ($k = 50$) satisfies all core design goals, exploring larger capacities reveals a complex failure mode. As k increases, we observe a sequential failure first in robustness (against adaptive attacks), then in stealthiness, and finally in fidelity as the main task collapses. Therefore, a viable k must be empirically validated against all three core properties simultaneously. A theoretical analysis of this complex relationship remains a direction for future work.

6. Discussion

Efficiency. Efficiency is another important metric, and Sigil is highly efficient due to its concise mechanism. Specifically, in our default setting ($k = 50$), the server-side overhead is minimal, requiring only $\approx 0.13\%$ additional computational load and $\approx 3\text{MB}$ of storage. Even at a high capacity of $k = 1000$, the computational overhead remains low at $\approx 2.6\%$, and storage is a modest $\approx 62.5\text{MB}$.

Robustness to Ambiguity Attacks. Furthermore, Sigil is inherently robust to ambiguity attacks. An adversary at-

TABLE 6. ABLATION STUDY ON SPLIT POINT STRATEGY (RESNET-18/CIFAR-10, $\lambda = 0.1$). ALL CELLS (EXCEPT SPLITOUT) SHOW TOP: ACC (%) / BOTTOM: WSR (%). THE SPLITOUT COLUMN SHOWS THE MEAN ANOMALY SAMPLES (LOWER IS BETTER).

Split Point	Fidelity		Stealthiness		Robustness						
	No Attack		SplitOut (\downarrow)		Training-time		Post-hoc			Adaptive Attack	
			Noise (snr=1/100)		FT (100 steps)	PR (80%)	QT (INT4)	$R_{wm}=10$	$R_{wm}=5$	$R_{wm}=2$	$R_{wm}=1$
Layer 1	92.4%	16.7	87.1%		91.3%	14.3%	90.1%	87.8%	85.1%	87.9%	89.7%
	99.8%		73.7%(-26.1)		99.8%	88.6%(-11.2)	99.8%	80.2%(-19.6)	80.4%(-19.4)	90.2%(-9.6)	99.3%(-0.5)
Layer 2	92.2%	20.44	79.9%		91.0%	10.0%	89.8%	86.7%	88.9%	88.7%	88.4%
	99.9%		96.3%(-3.6)		99.9%	97.5%(-2.4)	99.9%	74.2%(-25.7)	70.2%(-29.7)	74.6%(-25.3)	93.8%(-6.1)
Layer 3	92.4%	8.95	64.6%		91.5%	10.5%	91.4%	87.9%	88.1%	88.2%	88.7%
	100%		99.2%(-0.8)		100%	94.6%(-5.4)	100%	99.7%(-0.3)	99.6%(-0.4)	79.7%(-20.3)	86.1%(-13.9)
Layer 4	92.1%	0	39.5%		91.6%	14.6%	90.7%	90.7%	88.9%	89.3%	90.0%
	100%		99.5%(-0.5)		99.9%(-0.1)	94.8%(-5.2)	100%	80.2%(-19.8)	79.4%(-20.6)	80.4%(-19.6)	80.1%(-19.9)

TABLE 7. ABLATION STUDY ON WATERMARK LENGTH (K) (RESNET-18/CIFAR-10, $\lambda = 0.1$). ALL CELLS (EXCEPT SPLITOUT) SHOW TOP: ACC (%) / BOTTOM: WSR (%). THE SPLITOUT COLUMN SHOWS THE MEAN ANOMALY SAMPLES (LOWER IS BETTER).

Length (k)	Fidelity		Stealthiness		Robustness						
	No Attack		SplitOut (\downarrow)		Post-hoc			Adaptive Attack			
					FT (100 steps)	PR (80%)	QT (INT4)	$R_{wm}=10$	$R_{wm}=5$	$R_{wm}=2$	$R_{wm}=1$
k=50	92.4%	8.95	91.5%		10.5%	91.4%	87.9%	88.1%	88.2%	88.7%	
	100%		100%		94.6%(-5.4)	100%	99.7%(-0.3)	99.6%(-0.4)	79.7%(-20.3)	86.1%(-13.9)	
k=500	92.2%	37.41	90.9%		10.0%	89.2%	89.5%	86.4%	91.1%	89.3%	
	100%		100%		86.6%(-13.4)	100%	63.0%(-37.0)	83.2%(-16.8)	98.6%(-1.4)	99.3%(-0.7)	
k=1000	92.2%	65.41	91.0%		11.4%	89.7%	89.3%	88.8%	87.6%	89.6%	
	100%		100%		84.8%(-15.2)	100%	99.7%(-0.3)	63.3%(-36.7)	79.2%(-20.8)	98.0%(-2.0)	
k=2000	91.5%	165.4 (Not Alerted)	90.5%		10.0%	89.5%	88.4%	88.7%	89.4%	89.0%	
	100%		99.9%(-0.1)		85.9%(-14.1)	99.9%(-0.1)	98.2%(-1.8)	78.8%(-21.2)	70.0%(-30.0)	93.7%(-6.3)	
k=3000	91.7%	592.39 (Alerted)	90.7%		10.0%	87.0%	89.7%	90.4%	89.1%	87.8%	
	100%		99.8%(-0.2)		88.5%(-11.5)	99.9%(-0.1)	97.6%(-2.4)	99.5%(-0.5)	88.2%(-11.8)	76.3%(-23.7)	

tempting to embed a different watermark using the same mechanism would generate a matrix M' that is orthogonal to M with high probability. This makes it impossible to overwrite or invalidate the original watermark.

Limitations. First, Sigil is vulnerable to the feature permutation attack, designed specifically against existing activation schemes [33]. This attack permutes the neurons (channels) at the split point, invalidating the watermark while leaving the main task accuracy unaffected. This vulnerability poses a fundamental challenge to all activation-based watermarking schemes. A possible direction to address this challenge is to explore permutation-invariant embedding targets or extraction methods. For instance, this suggests designing more complex embedding objects, such as targeting higher-order statistics or using a dedicated DNN for recovery, an approach analogous to recent work in parameter watermarking [31].

Second, similar to most existing watermark schemes, Sigil is not robust against model extraction attacks. Model extraction removes the Sigil watermark precisely because this attack creates a new surrogate model that only mim-

ics the black-box functionality of the source model. Since Sigil's watermark is a white-box statistical property of the internal activation space, it is not part of the functionality that gets extracted. Integrating extraction-robust techniques with Sigil's server-enforced embedding in the U-SFL setting remains an open research problem.

7. Conclusion

In this paper, we investigate the key challenge of embedding verifiable model ownership evidence into a malicious client's model by a capability-limited server under U-SFL. We formalized this threat model, revealed the dilemma faced by traditional methods, and proposed Sigil, a general activation watermarking framework. We designed an adaptive gradient clipping mechanism and rigorously evaluated it against a targeted adaptive subspace removal attack. Extensive experimental evaluations on the Sigil framework fully validated its fidelity, robustness, and stealthiness. Our work provides a new solution for exploring the boundaries between privacy protection and ownership verification in decentralized machine learning.

Appendix A. Model Structure

The detailed architectures for the models used in our experiments are presented in the following tables. Our default U-SFL configuration splits each model at a specific intermediate layer. For ResNet-18, the default split point is after layer3. For VGG11, the split occurs after pool4. For MobileNetV2, the split is after layer_group6, and for DenseNet-121, it is after transition3.

TABLE 8. RESNET-18 ARCHITECTURE (FOR CIFAR-10, 32x32 INPUTS).

Layer	Block Details / Stride	Output Shape (Dim.)
Input	-	(3, 32, 32) (Dim: 3,072)
conv1	3x3 conv, 64, stride 1	(64, 32, 32) (Dim: 65,536)
bn1+relu	-	(64, 32, 32) (Dim: 65,536)
maxpool	Identity (per code)	(64, 32, 32) (Dim: 65,536)
layer1	[BasicBlock, 64] x 2 (stride = 1)	(64, 32, 32) (Dim: 65,536)
layer2	[BasicBlock, 128] x 2 (stride = 2)	(128, 16, 16) (Dim: 32,768)
layer3	[BasicBlock, 256] x 2 (stride = 2)	(256, 8, 8) (Dim: 16,384)
layer4	[BasicBlock, 512] x 2 (stride = 2)	(512, 4, 4) (Dim: 8,192)
avgpool	AdaptiveAvgPool (1x1)	(512, 1, 1) (Dim: 512)
flatten	-	(512) (Dim: 512)
fc	Linear (512, 10)	(10) (Dim: 10)

TABLE 9. VGG11 ARCHITECTURE (FOR CIFAR-10, 32x32 INPUTS).

Layer	Block Details / Stride	Output Shape (Dim.)
Input	-	(3, 32, 32) (Dim: 3,072)
stage1	[Conv 64]	(64, 32, 32) (Dim: 65,536)
pool1	MaxPool, stride 2	(64, 16, 16) (Dim: 16,384)
stage2	[Conv 128]	(128, 16, 16) (Dim: 32,768)
pool2	MaxPool, stride 2	(128, 8, 8) (Dim: 8,192)
stage3	[Conv 256] x 2	(256, 8, 8) (Dim: 16,384)
pool3	MaxPool, stride 2	(256, 4, 4) (Dim: 4,096)
stage4	[Conv 512] x 2	(512, 4, 4) (Dim: 8,192)
pool4	MaxPool, stride 2	(512, 2, 2) (Dim: 2,048)
stage5	[Conv 512] x 2	(512, 2, 2) (Dim: 2,048)
pool5	MaxPool, stride 2	(512, 1, 1) (Dim: 512)
avgpool	Identity (per code)	(512, 1, 1) (Dim: 512)
flatten	-	(512) (Dim: 512)
fc	Linear(512, 512) ...	(10) (Dim: 10)

Appendix B. Detailed Settings

Implementation Details. All experiments were conducted on a server running Ubuntu 22.04. We utilized a single NVIDIA RTX 5090 GPU for all training and evaluation.

TABLE 10. MOBILENETV2 ARCHITECTURE (FOR TINY-IMAGENET, 64x64 INPUTS).

Layer	Block Details / Stride	Output Shape (Dim.)
Input	-	(3, 64, 64) (Dim: 12,288)
conv1	3x3 conv, 32, stride 1	(32, 64, 64) (Dim: 131,072)
group1	InvertedResidual (t=1, c=16, n=1, s=1)	(16, 64, 64) (Dim: 65,536)
group2	InvertedResidual (t=6, c=24, n=2, s=2)	(24, 32, 32) (Dim: 24,576)
group3	InvertedResidual (t=6, c=32, n=3, s=2)	(32, 16, 16) (Dim: 8,192)
group4	InvertedResidual (t=6, c=64, n=4, s=2)	(64, 8, 8) (Dim: 4,096)
group5	InvertedResidual (t=6, c=96, n=3, s=1)	(96, 8, 8) (Dim: 6,144)
group6	InvertedResidual (t=6, c=160, n=3, s=2)	(160, 4, 4) (Dim: 2,560)
group7	InvertedResidual (t=6, c=320, n=1, s=1)	(320, 4, 4) (Dim: 5,120)
conv2	1x1 conv, 1280, stride 1	(1280, 4, 4) (Dim: 20,480)
avgpool	AdaptiveAvgPool (1x1)	(1280, 1, 1) (Dim: 1,280)
flatten	-	(1280) (Dim: 1,280)
fc	Linear (1280, 200)	(200) (Dim: 200)

TABLE 11. DENSENET-121 ARCHITECTURE (FOR TINY-IMAGENET, 64x64 INPUTS).

Layer	Block Details (Layers / Growth)	Output Shape (Dim.)
Input	-	(3, 64, 64) (Dim: 12,288)
conv_initial	7x7 conv, 64, stride 2	(64, 32, 32) (Dim: 65,536)
pool0	3x3 MaxPool, stride 2	(64, 16, 16) (Dim: 16,384)
block1	6 layers, g=32	(256, 16, 16) (Dim: 65,536)
trans1	1x1 conv + AvgPool, s=2	(128, 8, 8) (Dim: 8,192)
block2	12 layers, g=32	(512, 8, 8) (Dim: 32,768)
trans2	1x1 conv + AvgPool, s=2	(256, 4, 4) (Dim: 4,096)
block3	24 layers, g=32	(1024, 4, 4) (Dim: 16,384)
trans3	1x1 conv + AvgPool, s=2	(512, 2, 2) (Dim: 2,048)
block4	16 layers, g=32	(1024, 2, 2) (Dim: 4,096)
norm_final	BatchNorm + ReLU	(1024, 2, 2) (Dim: 4,096)
avgpool	AdaptiveAvgPool (1x1)	(1024, 1, 1) (Dim: 1,024)
flatten	-	(1024) (Dim: 1,024)
fc	Linear (1024, 200)	(200) (Dim: 200)

The implementation was built using Python 3.12, PyTorch 2.8.0, and CUDA 13.0.

Hyperparameter Settings. All models were trained for a total of 80 global communication rounds. In each round, every client performed $E = 2$ local epochs of training on its private data. We used a global batch size of 256.

For optimization, we employed the SGD optimizer with a momentum of 0.9 and weight decay of 5e-4. The learning rate schedule utilized a combination of a 5-round linear warmup followed by cosine annealing. The base learning

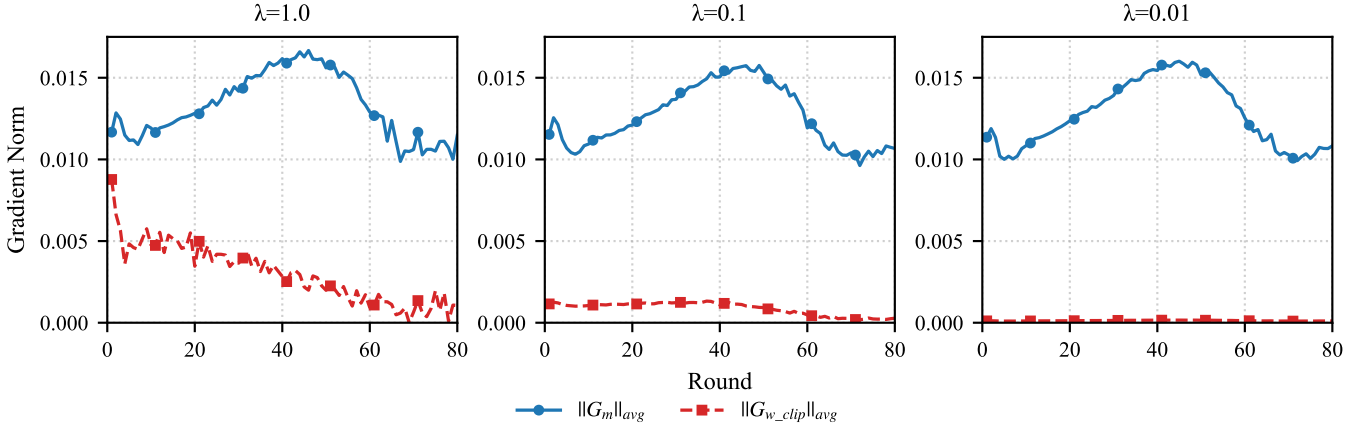


Figure 8. Visualization of gradient components during training (ResNet-18/CIFAR-10) under different watermark strength (λ) settings.

rate was set to 1×10^{-1} , and the learning rate annealed down to a minimum of 1×10^{-4} by the end of training.

Appendix C. Gradient Composition During Training

This section visualizes the relative magnitudes of the main task and watermark gradient components during the training process. Figure 8 plots the average L2 norms of the main task gradient ($\|G_m\|_{avg}$) and the clipped watermark gradient ($\|G_{w,clip}\|_{avg}$) over 80 global rounds for various λ settings on the ResNet-18/CIFAR-10 task. These plots visually confirm two key points:

- For strong λ values (e.g., $\lambda = 1.0$), the watermark gradient norm is significant during the early training phase and diminishes as the watermark becomes embedded. This provides the observable signal that the adaptive attack attempts to exploit.
- For our default ($\lambda = 0.1$) and stealthier ($\lambda = 0.01$) settings, the watermark gradient norm is consistently and significantly suppressed by our adaptive clipping mechanism, remaining much smaller than the main task gradient norm throughout training.

Appendix D. Mathematical Relation of Gradient, Projection, and Embedding Matrix

This appendix mathematically clarifies the theoretical foundation of the adaptive subspace removal attack detailed in Section 5.4.

The attack's effectiveness relies on two key mathematical relations:

- 1) The watermark gradient G_{wm} is confined to the subspace S_{wm} defined by the embedding matrix M .
- 2) The watermark information is encoded by the projection of the activation A_{flat} onto S_{wm} .

Therefore, the attacker can analyze G_{final} to estimate G_{wm} and then S_{wm} . In the ideal case, forcing the projection of A_{flat} onto S_{wm} to zero can precisely remove the watermark and leave the components of A_{flat} in other (main task) subspaces unaffected.

The following subsections provide the definitions and the mathematical derivation that underpin these two relations.

D.1 Definitions and Review

- $A_i^{(t)}$: The original activation tensor uploaded by client i at round t .
- $A_{flat} \in \mathbb{R}^{1 \times d}$: The flattened form of $A_i^{(t)}$, a row vector representing the activation carrier.
- d : The total dimension of A_{flat} (e.g., $d = 16,384$ in our default setting).
- $M \in \mathbb{R}^{d \times k}$: The server's secret watermark embedding matrix.
- $m_j \in \mathbb{R}^{d \times 1}$: The j -th column vector of the matrix M .
- $S_{wm} = \text{span}(m_1, \dots, m_k)$: The k -dimensional "Watermark Subspace" spanned by the column vectors of M .
- $P = A_{flat} \cdot M \in \mathbb{R}^{1 \times k}$: The projection of the activation onto the watermark subspace.
- $b \in \mathbb{R}^{1 \times k}$: The server's target bit string (row vector).
- \mathcal{L}_{wm} : The watermark loss function. Note that this loss is **only** a function of the watermark projection P :

$$\mathcal{L}_{wm} = \text{BCE}(\sigma(P), b). \quad (6)$$

- $G_{wm} \in \mathbb{R}^{1 \times d}$: The gradient of \mathcal{L}_{wm} with respect to A_{flat} (omitting i, t subscripts for clarity).

D.2 Derivation

To compute $G_{wm} = \frac{\partial \mathcal{L}_{wm}}{\partial A_{flat}}$, we apply the chain rule:

$$G_{wm} = \frac{\partial \mathcal{L}_{wm}}{\partial A_{flat}} = \frac{\partial \mathcal{L}_{wm}}{\partial P} \cdot \frac{\partial P}{\partial A_{flat}}. \quad (7)$$

The derivation requires computing the two partial derivative terms.

For the first term, $\frac{\partial \mathcal{L}_{wm}}{\partial P}$, which is the derivative of the loss with respect to the projection P . This yields a $1 \times k$ row vector, which we denote as the error coefficients C :

$$C = \frac{\partial \mathcal{L}_{wm}}{\partial P} = [c_1, c_2, \dots, c_k], \quad (8)$$

C is a $1 \times k$ coefficient vector representing the error.

For the second term, $\frac{\partial P}{\partial A_{flat}}$, which is the Jacobian and the derivative of $P = A_{flat}M$ with respect to A_{flat} . Based on the standard matrix calculus identity (if $y = xA$, then $\frac{\partial y}{\partial x} = A^T$), we get:

$$\frac{\partial P}{\partial A_{flat}} = M^T, \quad (9)$$

where $M^T \in \mathbb{R}^{k \times d}$ is the transpose of the embedding matrix M .

Substituting these terms back, we get the final expression for G_{wm} :

$$G_{wm} = C \cdot M^T = \sum_{j=1}^k c_j \cdot (m_j)^T, \quad (10)$$

where $(m_j)^T$ is the transpose of the j -th column vector m_j of M .

Conclusion: This derivation confirms the two relations stated in the introduction. The Gradient Confinement (Relation 1) is established by the equation $G_{wm} = \sum c_j (m_j)^T$, which explicitly shows that the watermark gradient G_{wm} is always a linear combination of the column vectors of M . Consequently, G_{wm} is mathematically confined to the watermark subspace S_{wm} . The Watermark Confinement (Relation 2) is confirmed by the definition in D.1, where the loss \mathcal{L}_{wm} is only a function of the projection $P = A_{flat} \cdot M$. This verifies that the watermark information is entirely encoded by this projection, completing the theoretical foundation for the adaptive attack.

Appendix E. Effectiveness of Sigil under Varied U-SFL Parameters

This section evaluates the impact of two U-SFL parameters on Sigil's effectiveness: the number of clients (c) and data heterogeneity, which encompasses both data distribution heterogeneity (Non-IID) and data quantity heterogeneity (Unbalanced).

E.1. Impact of Client Counts

Table 12 shows that for watermarking strengths $\lambda = 1$ and $\lambda = 0.1$, the WSR remains at 100%. At the weakest strength ($\lambda = 0.01$), the WSR exhibits a slight decline as c increases, reaching 89.0% at $c = 100$. We hypothesize this decline is due to insufficient embedding, a consequence

TABLE 12. SIGIL EFFECTIVENESS UNDER DIFFERENT CLIENT COUNTS(c) AND WATERMARK STRENGTHS λ . EACH CELL SHOWS TOP: ACC (%) / BOTTOM: WSR (%).

Client Counts	Watermark Strength λ		
	$\lambda = 1$	$\lambda = 0.1$	$\lambda = 0.01$
$c = 10$	92.8	92.4	92.4
	100.0	100.0	99.1(-0.9)
$c = 20$	89.8	88.9	89.8
	100.0	100.0	98.4(-1.6)
$c = 50$	83.9	84.4	84.2
	100.0	100.0	97.3(-2.7)
$c = 100$	74.1	73.8	72.1
	100.0	100.0	89.0(-11.0)

TABLE 13. WATERMARK EMBEDDING RESULTS UNDER DIFFERENT NON-IID LEVELS β AND WATERMARK STRENGTHS λ . EACH CELL SHOWS TOP: ACC (%) / BOTTOM: WSR (%).

Non-IID β	Watermark Strength λ		
	$\lambda = 1$	$\lambda = 0.1$	$\lambda = 0.01$
IID	92.8	92.4	92.4
	100.0	100.0	99.1(-0.9)
$\beta = 1.0$	90.8	91.3	90.6
	100.0	100.0	99.2(-0.8)
$\beta = 0.5$	90.1	90.5	88.9
	100.0	100.0	99.4(-0.6)
$\beta = 0.1$	66.3	77.2	70.9
	100.0	100.0	99.5(-0.5)

of the minimal data available per client at this low strength. Nevertheless, this WSR remains well above the 70% success threshold, even as Acc declines significantly (owing to the reduced data volume per client).

E.2. Data Heterogeneity

We evaluated the impact of two types of data heterogeneity:

- **Data Distribution Heterogeneity (Non-IID):** We simulate this using a Dirichlet distribution ($Dir(\beta)$). The parameter β controls the degree of Non-IID; a smaller β indicates greater disparity among clients. We test $\beta \in \{1.0, 0.5, 0.1\}$, where $\beta = 1.0$ represents a moderate skew and $\beta = 0.1$ represents extreme Non-IID (i.e., each client's data consists almost exclusively of one or two classes).
- **Data Quantity Heterogeneity (Unbalanced):** We simulate this by controlling the standard deviation σ of client sample sizes, which follows a log-normal distribution. A larger σ signifies a greater imbalance in data quantity across clients. We test $\sigma \in \{0.5, 1.0, 2.0\}$, where $\sigma = 0.5$ represents a slight fluctuation and $\sigma = 2.0$ indicates an extreme disparity in data volume (e.g., 10% of clients holding 60-80% of the data).

TABLE 14. WATERMARK EMBEDDING RESULTS UNDER DIFFERENT UNBALANCED LEVELS σ AND WATERMARK STRENGTHS λ . EACH CELL SHOWS TOP: ACC (%) / BOTTOM: WSR (%).

Unbalanced σ	Watermark Strength λ		
	$\lambda = 1$	$\lambda = 0.1$	$\lambda = 0.01$
Balanced	92.8	92.4	92.4
	100.0	100.0	99.1(-0.9)
$\sigma = 0.5$	92.5	92.4	92.5
	100.0	100.0	98.9(-1.1)
$\sigma = 1.0$	92.4	92.3	92.2
	100.0	100.0	99.2(-0.8)
$\sigma = 2.0$	92.2	92.6	92.2
	100.0	100.0	98.6(-1.4)

Tables 13 and 14 demonstrate that Sigil is highly robust to data heterogeneity. For all tested β (down to 0.1) and σ (up to 2.0) values, the WSR remains above 98%. This indicates that Sigil can reliably embed and verify watermarks despite skewed data class distributions or severe data quantity imbalances among clients.

In summary, this analysis confirms that Sigil remains effective under realistic U-SFL scenarios, including a large number of clients and severe data heterogeneity (in distribution and quantity), which demonstrates its practical feasibility.

References

- [1] K. He, X. Zhang, S. Ren, and J. Sun, “Deep residual learning for image recognition,” in *Proceedings of the IEEE Conference on Computer Vision and Pattern Recognition (CVPR)*, June 2016.
- [2] T. Chen, S. Kornblith, M. Norouzi, and G. E. Hinton, “A simple framework for contrastive learning of visual representations,” in *Proceedings of the 37th International Conference on Machine Learning, ICML 2020, 13-18 July 2020, Virtual Event*, ser. Proceedings of Machine Learning Research, vol. 119. PMLR, 2020, pp. 1597–1607. [Online]. Available: <http://proceedings.mlr.press/v119/chen20j.html>
- [3] A. Krizhevsky, I. Sutskever, and G. E. Hinton, “Imagenet classification with deep convolutional neural networks,” *Commun. ACM*, vol. 60, no. 6, pp. 84–90, 2017. [Online]. Available: <https://doi.org/10.1145/3065386>
- [4] M. Fredrikson, S. Jha, and T. Ristenpart, “Model inversion attacks that exploit confidence information and basic countermeasures,” in *Proceedings of the 22nd ACM SIGSAC Conference on Computer and Communications Security*, ser. CCS ’15. New York, NY, USA: Association for Computing Machinery, 2015, p. 1322–1333. [Online]. Available: <https://doi.org/10.1145/2810103.2813677>
- [5] F. Tramèr, F. Zhang, A. Juels, M. K. Reiter, and T. Ristenpart, “Stealing machine learning models via prediction APIs,” in *25th USENIX Security Symposium (USENIX Security 16)*. Austin, TX: USENIX Association, Aug. 2016, pp. 601–618. [Online]. Available: <https://www.usenix.org/conference/usenixsecurity16/technical-sessions/presentation/tramer>
- [6] Y. Adi, C. Baum, M. Cisse, B. Pinkas, and J. Keshet, “Turning your weakness into a strength: Watermarking deep neural networks by backdooring,” in *27th USENIX Security Symposium (USENIX Security 18)*. Baltimore, MD: USENIX Association, Aug. 2018, pp. 1615–1631. [Online]. Available: <https://www.usenix.org/conference/usenixsecurity18/presentation/adi>
- [7] P. Lv, H. Ma, K. Chen, J. Zhou, S. Zhang, R. Liang, S. Zhu, P. Li, and Y. Zhang, “Mea-defender: A robust watermark against model extraction attack,” in *2024 IEEE Symposium on Security and Privacy (SP)*, 2024, pp. 2515–2533.
- [8] Y. Uchida, Y. Nagai, S. Sakazawa, and S. Satoh, “Embedding watermarks into deep neural networks,” in *Proceedings of the 2017 ACM on International Conference on Multimedia Retrieval*, ser. ICMR ’17. New York, NY, USA: Association for Computing Machinery, 2017, p. 269–277. [Online]. Available: <https://doi.org/10.1145/3078971.3078974>
- [9] Y. Yan, X. Pan, M. Zhang, and M. Yang, “Rethinking White-Box watermarks on deep learning models under neural structural obfuscation,” in *32nd USENIX Security Symposium (USENIX Security 23)*. Anaheim, CA: USENIX Association, Aug. 2023, pp. 2347–2364. [Online]. Available: <https://www.usenix.org/conference/usenixsecurity23/presentation/yan>
- [10] T. Krauß, J. Stang, and A. Dmitrienko, “ClearStamp: A Human-Visible and robust Model-Ownership proof based on transposed model training,” in *33rd USENIX Security Symposium (USENIX Security 24)*. Philadelphia, PA: USENIX Association, Aug. 2024, pp. 5269–5286. [Online]. Available: <https://www.usenix.org/conference/usenixsecurity24/presentation/krauss-clearstamp>
- [11] B. McMahan, E. Moore, D. Ramage, S. Hampson, and B. A. y. Arcas, “Communication-Efficient Learning of Deep Networks from Decentralized Data,” in *Proceedings of the 20th International Conference on Artificial Intelligence and Statistics*, ser. Proceedings of Machine Learning Research, A. Singh and J. Zhu, Eds., vol. 54. PMLR, 20–22 Apr 2017, pp. 1273–1282. [Online]. Available: <https://proceedings.mlr.press/v54/mcmahan17a.html>
- [12] P. Kairouz, H. B. McMahan, B. Avent, A. Bellet, M. Bennis, A. N. Bhagoji, K. Bonawitz, Z. Charles, G. Cormode, R. Cummings, R. G. L. D’Oliveira, H. Eichner, S. E. Rouayheb, D. Evans, J. Gardner, Z. Garrett, A. Gascón, B. Ghazi, P. B. Gibbons, M. Gruteser, Z. Harchaoui, C. He, L. He, Z. Huo, B. Hutchinson, J. Hsu, M. Jaggi, T. Javidi, G. Joshi, M. Khodak, J. Konecny, A. Korolova, F. Koushanfar, S. Koyejo, T. Lepoint, Y. Liu, P. Mittal, M. Mohri, R. Nock, A. Özgür, R. Pagh, H. Qi, D. Ramage, R. Raskar, M. Raykova, D. Song, W. Song, S. U. Stich, Z. Sun, A. T. Suresh, F. Tramèr, P. Vepakomma, J. Wang, L. Xiong, Z. Xu, Q. Yang, F. X. Yu, H. Yu, and S. Zhao, “Advances and open problems in federated learning,” *Foundations and Trends® in Machine Learning*, vol. 14, no. 1–2, pp. 1–210, 2021. [Online]. Available: <http://dx.doi.org/10.1561/2200000083>
- [13] O. Gupta and R. Raskar, “Distributed learning of deep neural network over multiple agents,” *Journal of Network and Computer Applications*, vol. 116, pp. 1–8, 2018. [Online]. Available: <https://www.sciencedirect.com/science/article/pii/S1084804518301590>
- [14] P. Vepakomma, O. Gupta, T. Swedish, and R. Raskar, “Split learning for health: Distributed deep learning without sharing raw patient data,” *arXiv e-prints*, p. arXiv:1812.00564, Dec. 2018.
- [15] C. Thapa, M. A. P. Chamikara, S. Camtepe, and L. Sun, “Splitfed: When federated learning meets split learning,” in *Thirty-Sixth AAAI Conference on Artificial Intelligence, AAAI 2022, Thirty-Fourth Conference on Innovative Applications of Artificial Intelligence, IAAI 2022, The Twelfth Symposium on Educational Advances in Artificial Intelligence, EAAI 2022 Virtual Event, February 22 - March 1, 2022*. AAAI Press, 2022, pp. 8485–8493. [Online]. Available: <https://doi.org/10.1609/aaai.v36i8.20825>
- [16] C. Thapa and S. A. Camtepe, “Advancements of federated learning towards privacy preservation: from federated learning to split learning,” in *Federated Learning Systems: Towards Next-Generation AI*. Springer, 2021, pp. 79–109.
- [17] J. Li, X. Chen, L. Yang, A. S. Rakin, D. Fan, and C. Chakrabarti, “EMGAN: early-mix-gan on extracting server-side model in split federated learning,” in *Thirty-Eighth AAAI Conference on Artificial Intelligence, AAAI 2024, Thirty-Sixth Conference on Innovative Applications of Artificial Intelligence, IAAI 2024, Fourteenth*

Symposium on Educational Advances in Artificial Intelligence, EAAI 2014, February 20-27, 2024, Vancouver, Canada, M. J. Wooldridge, J. G. Dy, and S. Natarajan, Eds. AAAI Press, 2024, pp. 13545–13553. [Online]. Available: <https://doi.org/10.1609/aaai.v38i12.29258>

[18] B. Zeng, S. Luo, F. Yu, G. Yang, K. Zhao, and L. Wang, “Gan-based data reconstruction attacks in split learning,” *Neural Networks*, vol. 185, p. 107150, 2025. [Online]. Available: <https://www.sciencedirect.com/science/article/pii/S089360825000292>

[19] X. Gao and L. Zhang, “PCAT: Functionality and data stealing from split learning by Pseudo-Client attack,” in *32nd USENIX Security Symposium (USENIX Security 23)*. Anaheim, CA: USENIX Association, Aug. 2023, pp. 5271–5288. [Online]. Available: <https://www.usenix.org/conference/usenixsecurity23/presentation/gao>

[20] B. Li, L. Fan, H. Gu, J. Li, and Q. Yang, “Fedipr: Ownership verification for federated deep neural network models,” *IEEE Transactions on Pattern Analysis and Machine Intelligence*, vol. 45, no. 4, pp. 4521–4536, 2023.

[21] X. Liu, S. Shao, Y. Yang, K. Wu, W. Yang, and H. Fang, “Secure federated learning model verification: A client-side backdoor triggered watermarking scheme,” in *2021 IEEE International Conference on Systems, Man, and Cybernetics (SMC)*, 2021, pp. 2414–2419.

[22] W. Yang, S. Shao, Y. Yang, X. Liu, X. Liu, Z. Xia, G. Schaefer, and H. Fang, “Watermarking in secure federated learning: A verification framework based on client-side backdooring,” *ACM Trans. Intell. Syst. Technol.*, vol. 15, no. 1, Dec. 2023. [Online]. Available: <https://doi.org/10.1145/3630636>

[23] B. G. A. Tekgul, Y. Xia, S. Marchal, and N. Asokan, “Waffle: Watermarking in federated learning,” in *2021 40th International Symposium on Reliable Distributed Systems (SRDS)*, 2021, pp. 310–320.

[24] S. Shao, W. Yang, H. Gu, Z. Qin, L. Fan, Q. Yang, and K. Ren, “Fedtracker: Furnishing ownership verification and traceability for federated learning model,” *IEEE Transactions on Dependable and Secure Computing*, vol. 22, no. 1, pp. 114–131, 2025.

[25] H. Jia, C. A. Choquette-Choo, V. Chandrasekaran, and N. Papernot, “Entangled watermarks as a defense against model extraction,” in *30th USENIX Security Symposium (USENIX Security 21)*. USENIX Association, Aug. 2021, pp. 1937–1954. [Online]. Available: <https://www.usenix.org/conference/usenixsecurity21/presentation/jia>

[26] S. Shao, Y. Li, H. Yao, Y. He, Z. Qin, and K. Ren, “Explanation as a watermark: Towards harmless and multi-bit model ownership verification via watermarking feature attribution,” in *32nd Annual Network and Distributed System Security Symposium, NDSS 2025, San Diego, California, USA, February 24-28, 2025*. The Internet Society, 2025. [Online]. Available: <https://doi.org/10.14722/ndss.2025.230338>

[27] J. Zhang, Z. Gu, J. Jang, H. Wu, M. P. Stoecklin, H. Huang, and I. Molloy, “Protecting intellectual property of deep neural networks with watermarking,” in *Proceedings of the 2018 on Asia Conference on Computer and Communications Security*, ser. ASIACCS ’18. New York, NY, USA: Association for Computing Machinery, 2018, p. 159–172. [Online]. Available: <https://doi.org/10.1145/3196494.3196550>

[28] H. Chen, B. Darvish Rohani, and F. Koushanfar, “DeepMarks: A Digital Fingerprinting Framework for Deep Neural Networks,” *arXiv e-prints*, p. arXiv:1804.03648, Apr. 2018.

[29] H. Liu, Z. Weng, and Y. Zhu, “Watermarking deep neural networks with greedy residuals,” in *Proceedings of the 38th International Conference on Machine Learning, ICML 2021, 18-24 July 2021, Virtual Event*, ser. Proceedings of Machine Learning Research, M. Meila and T. Zhang, Eds., vol. 139. PMLR, 2021, pp. 6978–6988. [Online]. Available: <http://proceedings.mlr.press/v139/liu21x.html>

[30] T. Wang and F. Kerschbaum, “Riga: Covert and robust white-box watermarking of deep neural networks,” in *Proceedings of the Web Conference 2021*, ser. WWW ’21. New York, NY, USA: Association for Computing Machinery, 2021, p. 993–1004. [Online]. Available: <https://doi.org/10.1145/3442381.3450000>

[31] P. Lv, P. Li, S. Zhang, K. Chen, R. Liang, H. Ma, Y. Zhao, and Y. Li, “A robustness-assured white-box watermark in neural networks,” *IEEE Transactions on Dependable and Secure Computing*, vol. 20, no. 6, pp. 5214–5229, 2023.

[32] B. Darvish Rohani, H. Chen, and F. Koushanfar, “Deepsigns: An end-to-end watermarking framework for ownership protection of deep neural networks,” in *Proceedings of the Twenty-Fourth International Conference on Architectural Support for Programming Languages and Operating Systems*, ser. ASPLOS ’19. New York, NY, USA: Association for Computing Machinery, 2019, p. 485–497. [Online]. Available: <https://doi.org/10.1145/3297858.3304051>

[33] N. Lukas, E. Jiang, X. Li, and F. Kerschbaum, “Sok: How robust is image classification deep neural network watermarking?” in *2022 IEEE Symposium on Security and Privacy (SP)*, 2022, pp. 787–804.

[34] D. Pasquini, G. Ateniese, and M. Bernaschi, “Unleashing the tiger: Inference attacks on split learning,” in *Proceedings of the 2021 ACM SIGSAC Conference on Computer and Communications Security*, ser. CCS ’21. New York, NY, USA: Association for Computing Machinery, 2021, p. 2113–2129. [Online]. Available: <https://doi.org/10.1145/3460120.3485259>

[35] F. Yu, B. Zeng, K. Zhao, Z. Pang, and L. Wang, “Chronic poisoning: Backdoor attack against split learning,” in *Thirty-Eighth AAAI Conference on Artificial Intelligence, AAAI 2024, Thirty-Sixth Conference on Innovative Applications of Artificial Intelligence, IAAI 2024, Fourteenth Symposium on Educational Advances in Artificial Intelligence, EAAI 2014, February 20-27, 2024, Vancouver, Canada*, M. J. Wooldridge, J. G. Dy, and S. Natarajan, Eds. AAAI Press, 2024, pp. 16531–16538. [Online]. Available: <https://doi.org/10.1609/aaai.v38i15.29591>

[36] B. Tajalli, O. Ersoy, and S. Picek, “On feasibility of server-side backdoor attacks on split learning,” in *2023 IEEE Security and Privacy Workshops (SPW)*, 2023, pp. 84–93.

[37] E. Erdogan, A. Küpcü, and A. E. Cicek, “Splitguard: Detecting and mitigating training-hijacking attacks in split learning,” in *Proceedings of the 21st Workshop on Privacy in the Electronic Society*, ser. WPES’22. New York, NY, USA: Association for Computing Machinery, 2022, p. 125–137. [Online]. Available: <https://doi.org/10.1145/3559613.3563198>

[38] J. Fu, X. Ma, B. B. Zhu, P. Hu, R. Zhao, Y. Jia, P. Xu, H. Jin, and D. Zhang, “Focusing on pinocchio’s nose: A gradients scrutinizer to thwart split-learning hijacking attacks using intrinsic attributes,” in *30th Annual Network and Distributed System Security Symposium, NDSS 2023, San Diego, California, USA, February 27 - March 3, 2023*. The Internet Society, 2023. [Online]. Available: <https://doi.org/10.14722/ndss.2023.24874>

[39] E. Erdogan, U. Teksen, M. S. Celiktenyildiz, A. Küpcü, and A. E. Cicek, “Splitout: Out-of-the-box training-hijacking detection in split learning via outlier detection,” in *International Conference on Cryptology and Network Security*. Springer, 2024, pp. 118–142.

[40] R. Vershynin, *High-Dimensional Probability: An Introduction with Applications in Data Science*, 2nd ed. Cambridge University Press, 2025, pre-publication draft dated October 24, 2025. Available at <https://www.math.uci.edu/~rvershyn/>. [Online]. Available: <https://www.math.uci.edu/~rvershyn/>

[41] Y. Mao, Z. Xin, Z. Li, J. Hong, Q. Yang, and S. Zhong, “Secure split learning against property inference, data reconstruction, and feature space hijacking attacks,” in *European Symposium on Research in Computer Security*. Springer, 2023, pp. 23–43.

[42] G. Gawron and P. Stubbings, “Feature Space Hijacking Attacks against Differentially Private Split Learning,” *arXiv e-prints*, p. arXiv:2201.04018, Jan. 2022.